View Online / Journal Homepage
Dynamic Article Links

Lab on a Chip

Cite this: DOI: 10.1039/c2lc21263c

www.rsc.org/loc

PAPER

Experimental validation of plugging during drop formation in a T-junction†

Adam R. Abate,*[ab] Pascaline Mary,[a] Volkert van Steijn[a] and David A. Weitz[a]

Received 16th December 2011, Accepted 14th February 2012
DOI: 10.1039/c2lc21263c

At low capillary number, drop formation in a T-junction is dominated by interfacial effects: as the dispersed fluid flows into the drop maker nozzle, it blocks the path of the continuous fluid; this leads to a pressure rise in the continuous fluid that, in turn, squeezes on the dispersed fluid, inducing pinch-off of a drop. While the resulting drop volume predicted by this "squeezing" mechanism has been validated for a range of systems, as of yet, the pressure rise responsible for the actual pinch-off has not been observed experimentally. This is due to the challenge of measuring the pressures in a T-junction with the requisite speed, accuracy, and localization. Here, we present an empirical study of the pressures in a T-junction during drop formation. Using Laplace sensors, pressure probes we have developed, we confirm the central ideas of the squeezing mechanism; however, we also uncover other findings, including that the pressure of the dispersed fluid is not constant but rather oscillates in anti-phase with that of the continuous fluid. In addition, even at the highest capillary number for which monodisperse drops can be formed, pressure oscillations persist, indicating that drop formation in confined geometries does not transition to an entirely shear-driven mechanism, but to a mechanism combining squeezing and shearing.

Introduction

Microfluidic devices are unsurpassed in their ability to structure fluids by forming monodisperse emulsions—collections of drops in an immiscible carrier fluid that are identical to less than 5% in diameter.[1–4] They can also form drops at incredibly fast rates—beyond 100 000 per second for some formulations and drop sizes.[5] This combination of extreme speed and unsurpassed control has made microfluidic drop formation useful for a spectrum of applications, from materials synthesis through the creation of microparticles and capsules,[6–12] to ultrahigh-throughput chemical and biological studies in which the drops are used as "reactors" for protein crystallization, DNA sequencing, and directed evolution.[13–16]

An important technique for forming drops in microfluidics is T-junction drop formation.[17] In this approach, the drops are formed by injecting the dispersed and continuous fluids into a T-shaped channel such that the dispersed fluid enters from the stem of the T and the continuous fluid from one arm of the T; the fluids exit through the other arm, as illustrated in Fig. 1a and 1b. The formation of a drop starts with the dispersed fluid invading the outlet arm of the T, restricting the flow path of the continuous fluid. This causes the pressure of the continuous fluid upstream to rise, pushing the dispersed fluid downstream and squeezing on its trailing interface. This creates a "neck" of fluid connecting the forming drop to the stem of the T. As the pressure of the continuous fluid increases due to the continued plugging of the outlet by the dispersed fluid, it squeezes on the neck, causing it to narrow and break. This releases a drop into the outlet, at which point the cycle repeats.

The formation of drops in a T-junction thus depends on the evolution of the pressures in the device. Based on a qualitative description of these pressures, a scaling law has been developed that properly explains the dependence of the drop volume on the ratio of the flow rates of the dispersed and continuous fluids.[18] While this scaling has been confirmed and extended to a predictive model describing the dependence of the drop volume on the geometry of the T-junction,[19] as of yet, the actual squeezing mechanism responsible for the droplet pinch-off has only been observed in simulations,[20] but never in experiments. This lack of direct experimental evidence of the mechanism is due to the challenging nature of measuring the pressures in a microfluidic device with the accuracy (Pascal), speed (microseconds) and localization (microns) required.

In this paper, we present an empirical study of the pressure fluctuations generated during drop formation in a microfluidic T-junction. Using Laplace sensors, pressure probes we have developed that allow accurate measurement of the local pressure in a microchannel with high temporal resolution, we confirm the central ideas of the squeezing mechanism: as the dispersed fluid

[a]*School of Engineering and Applied Sciences and Department of Physics, Harvard University, Cambridge, Massachusetts, USA*
[b]*Department of Bioengineering and Therapeutic Sciences and California Institute for Quantitative Biosciences, University of California, San Francisco, California, USA. E-mail: adam.abate@ucsf.edu*
† Electronic supplementary information (ESI) available: High-speed camera movies of drop formation in a T-junction with Laplace sensors. See DOI: 10.1039/c2lc21263c

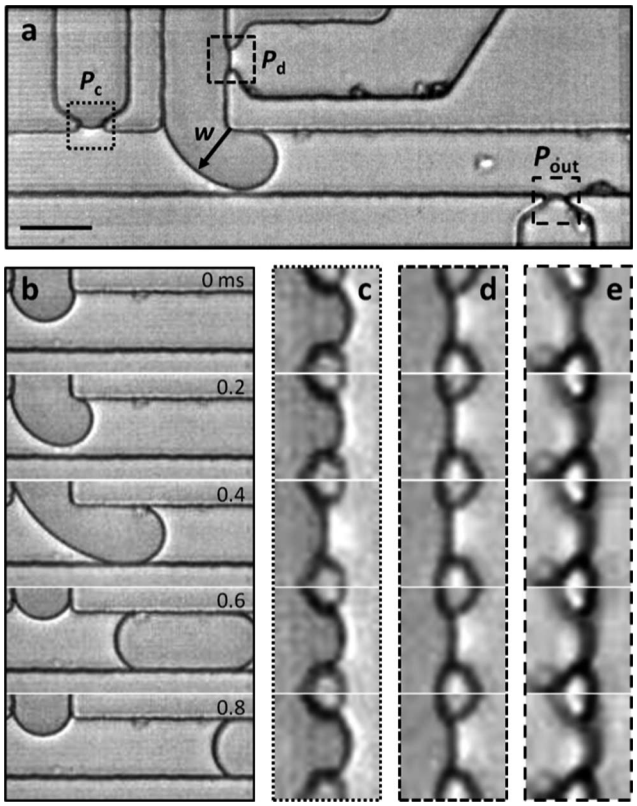

Fig. 1 (a) T-junction drop maker with three Laplace sensors used to measure the pressures in the continuous fluid upstream of the drop maker P_c, downstream of the drop maker P_{out} and in the dispersed fluid P_d. Scale bar: 25 μm. (b) Image sequence showing the evolution of the formation of a drop and (c–e) simultaneous snapshots of the interfaces at the Laplace sensors at high magnification. This device allows us to directly compare the evolution of the drop interface with the pressures at the three Laplace sensors.

flows into the drop maker, it induces a pressure rise in the continuous fluid that is responsible for drop pinch-off. However, we also uncover other findings. In contrast to common assumptions, the pressure in the dispersed fluid is not constant but rather oscillates in anti-phase with that of the continuous fluid. In addition, as the capillary number (Ca) of the flow is increased, the system does not transition to a fully shear-driven mechanism; instead, even at the highest Ca at which our device forms monodisperse drops, we observe pressure fluctuations indicative of plugging and squeezing. This indicates that the system approaches a mechanism combining squeezing and shearing.

Materials and methods

Materials

Our microfluidic devices are fabricated using soft lithography in (poly)dimethylsiloxane.[21] The devices consist of a T-junction drop maker with channel dimensions of 25 μm in width and height. To form water-in-oil emulsions, we make our devices hydrophobic by treating them with Aquapel. We flow a few microlitres of Aquapel through the devices and blow them dry with air. The devices are then baked in an oven set to 65 °C for 1 h, after which they are ready to use. For the droplet fluid we use de-ionized water and for the continuous fluid the fluorinated oil HFE-7500, having a viscosity of 1.2 mPa s, which is close to that of water. We also use the ammonium carboxylate salt of Krytox FSL at 2 wt% as a surfactant, to reduce interfacial tension and stabilize the drops. With this combination of solutions, we measure an interfacial tension of ~4 mN m^{-1}.

The Laplace sensor

The purpose of the Laplace sensor is to allow us to measure the time-dependent local pressure in a microchannel without perturbing the flow in the microchannel. There are many problems in microfluidics that require fast, accurate, and *localized* measurement of pressure,[22–28] a particularly good example of which is T-junction drop formation.[2,18,19] To enable such a measurement, Laplace sensors consist of two channels intersecting at a T: a test channel in which the pressure is to be measured, and a sensor channel in which the pressure is controlled. The sensor channel at the stem of the T is initially wide but abruptly narrows to an orifice of ~8 μm where it intersects the test channel, as shown by the Laplace sensor P_c in Fig. 1a. To measure the pressure in the test channel (in the lower-half of the dashed box shown in the figure), we introduce a sensor fluid into the sensor channel. The sensor fluid is immiscible with the test fluid, causing an interface between them to form that is cradled in the narrow orifice of the Laplace sensor, as illustrated in Fig. 1a. In such a geometry, the pressure of the test fluid P_1 is related to the pressure of the sensor fluid P_2 through the Laplace law,

$$P_1 - P_2 = 2\gamma/r, \quad (1)$$

with γ the interfacial tension of the interface and r its radius of curvature. This simple relationship allows us to measure the pressure in the test channel by imaging the curvature of the liquid interface. If the pressure difference between the test and sensor channels is small, the interface adopts a flattened shape characterized by a large radius of curvature; however, if the difference is large, the interface bulges far into the test channel, adopting a more curved shape with a smaller radius of curvature. By fixing the pressure in the sensor channel P_2, the interface thus becomes an optical probe of the pressure in the microchannel, bending inward and outward in response to fluctuations in pressure. Importantly, the interface of the Laplace sensor equilibrates fast compared to the timescales that govern drop formation, so that the pressure measurement is effectively instantaneous.[29] To confirm this, we estimate the Weber number (We) of the sensing fluid during a large pressure fluctuation producing a rapid movement of the interface. Even for the largest fluctuations we observe We < 10^{-2}, indicating that inertial stresses are small compared to interfacial ones.

We record the motion of the interfaces with a Phantom V7 fast camera at a frame rate of 31,250 fps and analyze the movies using LabVIEW's Vision image-analysis toolkit. The radius of curvature is obtained by identifying the contour of the interface and fitting it to a semi-circle, as shown for examples of low and high pressure differences in Fig. 2. To simplify the fit, we use the

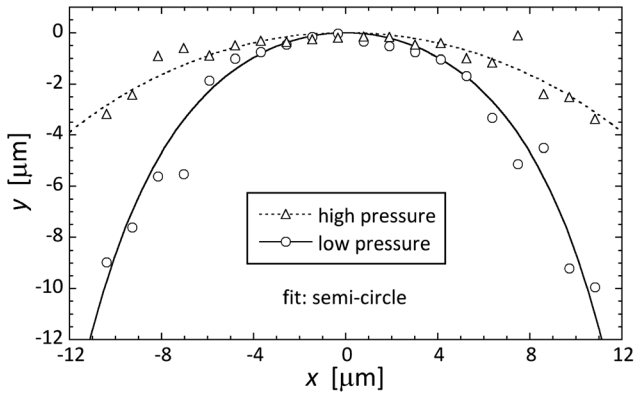

Fig. 2 x–y position of the contour of the interface of the P_c Laplace sensor, as determined by image analysis. Contours for two examples are shown, corresponding to low (high radius of curvature) and high (low radius of curvature) pressure differences. To determine these differences, the contours are fit to the Taylor series expansion of a semi-circle truncated to 6th order. The fit returns the radius of curvature, r, which best describes the data, which we then use *via* the Laplace law to measure the pressures in the microchannel. Fit: Taylor series of $y = (r^2 - x^2)^{1/2} - r$ to 6th order.

Taylor series expansion of a semi-circle truncated to 6th order; the only fit parameter in the resultant polynomial is the radius-of-curvature. Using the measured radius-of-curvature, the control pressure of the sensor channel, and the interfacial tension between our fluids, we calculate the absolute pressure in the test channel, just on the other side of the Laplace sensor interface.

Laplace sensors have several advantages for microfluidic characterization over other pressure sensors. Whereas pressure sensors available for purchase can be used to measure pressure-drops through microchannels, Laplace sensors afford *local* measurements of the *absolute* pressure in a microchannel, which is critical for characterizing the fluctuations generated during drop formation. Moreover, in contrast to methods that utilize comparator channels containing a miscible fluid to measure pressure,[22,26] in Laplace sensors, the sensing fluid is immiscible with the test fluid; this prevents transfer between these fluids, minimally perturbing the process under investigation. Finally, Laplace sensors are unsurpassed in their speed, sensitivity, and the ease with which they can be integrated into a microfluidic device, since the sensor is an orifice spanning only a few microns in width. In our study of drop formation, this allows us to integrate three sensors at different positions within the very small drop maker, which would be impractical with other pressure sensors.

Quantifying pressure fluctuations in a T-junction

To use Laplace sensors to characterize the pressure fluctuations generated during drop formation in a T-junction, we place three of them at different locations in the drop maker. To test the central idea of the squeezing mechanism,[18] that the plugging of the drop maker nozzle by the dispersed fluid causes a pressure rise in the continuous fluid upstream, we place a sensor just upstream of the T-junction on the continuous fluid inlet, as indicated by P_c in Fig. 1a. To confirm whether the dispersed fluid pressure is constant during drop-formation, as is commonly assumed, we place a sensor on the inlet of this fluid, as shown by P_d. Finally, to determine whether the pressure fluctuates downstream of the drop maker, we place a third sensor there, as shown by P_{out} in Fig. 1a. We fill the Laplace sensor in the dispersed fluid channel with the same oil and surfactant solution used to make drops, while de-ionized water is used for the other two sensors. Each Laplace sensor is independently pressurized using its own regulator, allowing us to tune each to the pressure at which its interface is in mechanical equilibrium.

Results and discussion

Pressure-fluctuation time traces

To measure the pressure fluctuations generated during drop formation, we image the evolution of the forming drop and, simultaneously, the motion of the Laplace sensor interfaces (see supplemental movies†). Early in the drop formation cycle the dispersed fluid flows into the main channel restricting the path of the continuous fluid, as shown for $t = 0$ to 0.4 ms in Fig. 1b. This coincides with a flattening of the interface of the P_c sensor, indicating a pressure increase upstream of the forming drop; simultaneously, the interface of the P_d sensor flattens, indicating a pressure decrease in the dispersed fluid. As the emerging drop continues forward, the curvature of the trailing interface inverts, transitioning from a convex to a concave shape; shortly thereafter, the interface narrows and breaks, forming a drop at $t =$ 0.6 ms. Concurrent with this is a rapid movement outward of the P_c interface, indicating a fall in pressure, as well as pronounced changes in P_d and P_{out}, indicating pressure changes in these regions as well, as shown in Fig. 1c–e.

To quantify the dynamics of the pressure fluctuations during drop formation, we analyze each frame in the high-speed camera movie. We measure the curvatures of the interfaces at the three sensors and calculate the corresponding pressures using the Laplace law (eqn (1)). By combining the measurements for all movie frames, we obtain three pressure traces as a function of time, one for each sensor. To relate these pressure dynamics to the drop formation dynamics, we also track the motion of the emerging drop. Using image analysis techniques we identify the location of the interface trailing behind the forming drop. We measure the narrowest width of the fluid neck, $w(t)$, corresponding to the shortest distance of the interface to the corner of the T-junction, as indicated in Fig. 1a.

The drop formation cycle starts when the dispersed fluid flows into the main channel. As the drop grows, it begins obstructing the main channel, restricting the flow path of the continuous fluid. As this happens, we observe a gradual increase in the continuous fluid upstream pressure P_c, as shown in Fig. 3b. The width $w(t)$ is constant during this stage, indicating that squeezing has not yet begun. Once the emerging drop fully plugs the main channel, the continuous fluid squeezes on the dispersed fluid, causing $w(t)$ to decrease linearly in time, as shown in Fig. 3a. The upstream pressure rises rapidly during this stage, reaching a maximum at the moment that the continuous phase fully engulfs the fluid neck, such that the neck lifts off of the top and bottom walls of the channel. The upstream pressure then decreases rapidly as the neck contracts inward, until the moment it breaks and a drop is released. The upstream pressure then

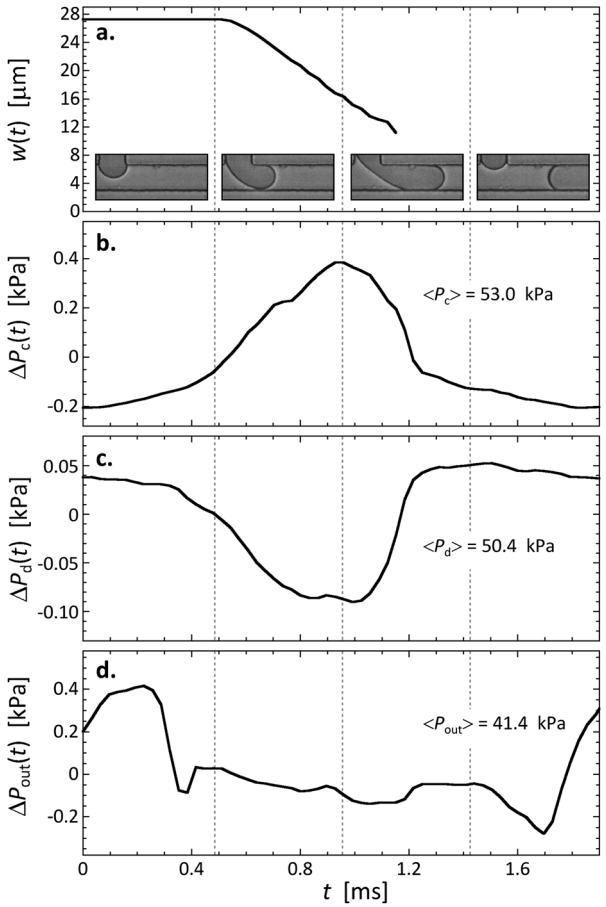

Fig. 3 Time-dependent measurements of (a) the emerging drop contour width at its narrowest point as indicated in Fig. 1a, the pressure fluctuation $\Delta P_i(t) = P_i(t) - \langle P_i \rangle$ for the (b) continuous and (c) dispersed fluids upstream of the T-junction, and (d) the continuous fluid downstream of the T-junction. As the emerging tip of the dispersed fluid blocks the nozzle, the pressure in the continuous fluid increases, bending the drop interface inward and eventually inducing pinch-off. These fluctuations are in anti-phase with the fluctuations in the dispersed fluid, which have a smaller amplitude. The final pinch off is signified by rapid pressure swings in both fluids, as well as a small bump in the outlet sensor.

gradually approaches the value corresponding to the start of the next cycle.

We measure the pressure P_d in the dispersed fluid using the same procedure. Interestingly, this pressure fluctuates in anti-phase with the upstream pressure, with an amplitude roughly five times smaller, as shown in Fig. 3c. The fluctuations of the downstream pressure P_{out} are also much smaller than those of the upstream pressure, except for the instant that the drop flows over this sensor, which is shown at the very start and end of the periodic cycle in Fig. 3d.

Dependence on the capillary number

One of the defining features of drop formation in the squeezing regime is that the interface is treated quasi-statically, meaning that it takes the shape that yields the minimum interfacial energy in each time instant.[29] This description is valid provided flow stresses are small compared to interfacial stresses, which is typically taken to be when Ca < 0.01. For increasing values of Ca, flow stresses become important and drop formation transitions from squeezing to a mechanism dominated by viscous shear.[18,20,30] A method often used to characterize this transition is to measure the dependence of the drop volume on Ca; however, such curves do not always show a sharp transition making it difficult to unequivocally determine the critical Ca.[31] A more direct way to characterize the transition is to use the scaling of the pressure fluctuations, which have been shown in simulations to be virtually independent of Ca in the squeezing regime, but fall off sharply with increasing Ca in the shearing regime.[20]

To characterize the transition between squeezing and shearing, we monitor the pressure fluctuations in our device while gradually increasing Ca. We focus on fluctuations in the P_c sensor for this investigation, because they are the largest and thus easiest to accurately measure, though we observe similar changes in the other sensors. At low Ca we observe large fluctuations in the continuous fluid, as expected for squeezing and shown for Ca = 0.03 in Fig. 4. When we double Ca we increase viscous forces relative to interfacial forces by a factor of two; however, the amplitudes of the pressure fluctuations hardly change and, rather, the frequency speeds up, as shown for Ca = 0.07. If, however, we double Ca again, shear begins to play a role: the pressure fluctuation amplitude decreases with increasing Ca, as shown in Fig. 4. This point marks the transition from drop formation described almost entirely by squeezing to one in which shearing and squeezing are both important. If Ca is increased yet again the fluctuations diminish even more, as shown for Ca = 0.21. At this value of Ca the system is very close to the jetting transition,[1,32] representing the highest values at which monodisperse drops can be formed in our device. Yet, pressure fluctuations persist indicating that squeezing still plays a role.

To characterize these qualitative changes we plot the amplitudes and characteristic timescales of the pressure fluctuations as

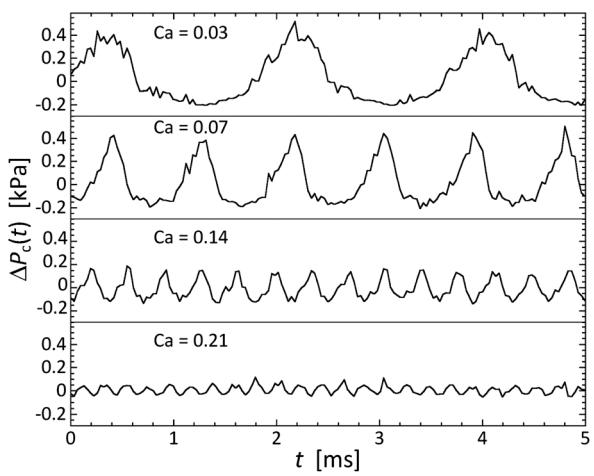

Fig. 4 Fluctuations as measured with P_c for different values of Ca. At low Ca, the fluctuations are most pronounced (0.03); by increasing Ca the fluctuations become more rapid but do not significantly diminish in amplitude (0.07). Increasing Ca causes viscous stresses to become important, resulting in diminished fluctuation amplitude (0.14). However, even at the highest Ca at which monodisperse drop formation is possible in our device (0.21), fluctuations persist, indicating that squeezing is always present in drop formation in confined channels.

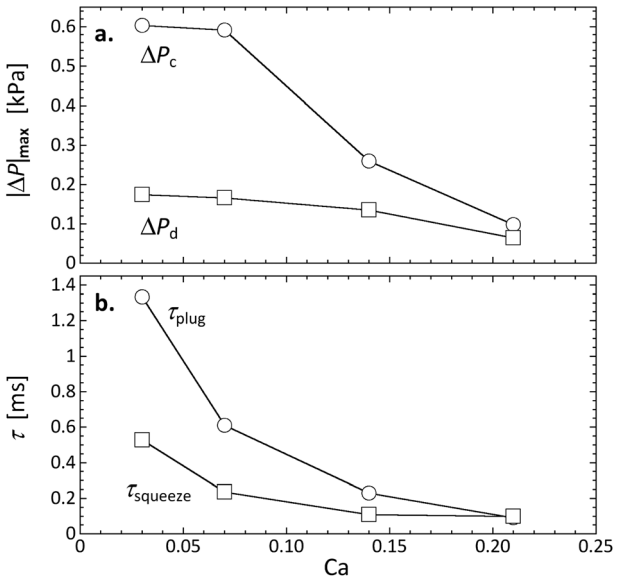

Fig. 5 Scaling of (a) pressure fluctuation amplitude and (b) plugging and squeezing durations as a function of Ca. The amplitudes are measured from the minimum and maximum of the pressure time traces, averaged over ~100 cycles. The plugging time is measured from the full-width, half-height of the valley in the fluctuation, and the squeezing time from that of the peak in the fluctuation.

a function of Ca, see Fig. 5. For the pressure amplitudes (Fig. 5a) we use the continuous and dispersed fluid pressures, and for the timescales (Fig. 5b) the duration of the fluctuation valley at half-min, full-width (the "plugging time") and the duration of the peak at half-max, full-width (the "squeezing time"),[20] both for the continuous fluid. For Ca $\leq$ 0.07, the fluctuation amplitude is roughly constant and changing flow conditions changes the drop formation frequency. The region 0.07 < Ca < 0.14 marks the transition in which the amplitudes begin to diminish rapidly but the peak and valley durations diminish more slowly. By Ca $\geq$ 0.21 we achieve a consistent state in which the amplitudes do not diminish much in size and the plugging and squeezing times are roughly equal. The transition value of 0.07 is ~5 times higher than what has been reported in the literature; this may indicate that the interface of our forming drops is not fully saturated with surfactant, such that the interfacial tension is larger than the equilibrium value used to calculate Ca. The left half of the plot thus corresponds to the squeezing mechanism while the right half to a scenario where shear is more important but squeezing still plays a role.

Conclusions

We have used Laplace sensors to perform a detailed analysis of the pressure fluctuations generated during drop formation in a microfluidic T-junction. Our results have allowed us to empirically validate the mechanism of plugging/squeezing drop formation. In addition, we discover that common assumptions of the process, including that the pressure in the dispersed fluid is constant during the formation cycle and that at high Ca the system transitions to a purely shear-driven mechanism, are incorrect. In fact, the pressure of the dispersed fluid fluctuates in anti-phase with that of the continuous fluid, and these fluctuations persist even at high Ca. These observations should be included in more detailed models of microfluidic drop formation in confined geometries. In particular, the fact that the pressure of the dispersed fluid is not constant should inform models seeking to describe the time-dependent shape evolution of the interface of the forming drop. Our results also validate the notion that the scaling of the pressure-fluctuation amplitudes with Ca is a good metric by which the importance of shearing or squeezing in a given drop maker can be judged. The Laplace sensors themselves should be useful for studies of other drop makers, like cross-junction, flow focus, and multiple emulsion drop makers.[1,3,11] They should also be useful more generally, essentially, whenever there is a need to measure the localized pressures in a microfluidic device with high accuracy and temporal resolution.

Acknowledgements

We thank Tobias Schneider for helpful discussions. This work was supported by the NSF (DMR-0602684), the Harvard MRSEC (DMR-0820484), and the Massachusetts Life Sciences Center.

Notes and references

1 S. L. Anna, N. Bontoux and H. A. Stone, *Appl. Phys. Lett.*, 2003, **82**, 364.
2 T. Thorsen, R. W. Roberts, F. H. Arnold and S. R. Quake, *Phys. Rev. Lett.*, 2001, **86**, 4163.
3 P. B. Umbanhowar, V. Prasad and D. A. Weitz, *Langmuir*, 2000, **16**, 347.
4 A. S. Utada, L. Y. Chu, A. Fernandez-Nieves, D. R. Link, C. Holtze and D. A. Weitz, *MRS Bull.*, 2007, **32**, 702.
5 A. R. Abate and D. A. Weitz, *Lab Chip*, 2011, **11**, 1911.
6 E. Lorenceau, A. S. Utada, D. R. Link, G. Cristobal, M. Joanicot and D. A. Weitz, *Langmuir*, 2005, **21**, 9183.
7 Z. H. Nie, S. Q. Xu, M. Seo, P. C. Lewis and E. Kumacheva, *J. Am. Chem. Soc.*, 2005, **127**, 8058.
8 D. Dendukuri, K. Tsoi, T. A. Hatton and P. S. Doyle, *Langmuir*, 2005, **21**, 2113.
9 L. Y. Chu, A. S. Utada, R. K. Shah, J. W. Kim and D. A. Weitz, *Angew. Chem., Int. Ed.*, 2007, **46**, 8970.
10 R. K. Shah, H. C. Shum, A. C. Rowat, D. Lee, J. J. Agresti, A. S. Utada, L. Y. Chu, J. W. Kim, A. Fernandez-Nieves, C. J. Martinez and D. A. Weitz, *Mater. Today*, 2008, **11**, 18.
11 A. R. Abate and D. A. Weitz, *Small*, 2009, **5**, 2030.
12 A. R. Abate, M. Kutsovsky, S. Seiffert, M. Windbergs, L. F. V. Pinto, A. Rotem, A. S. Utada and D. A. Weitz, *Adv. Mater.*, 2011, **23**, 1757.
13 B. Zheng, J. D. Tice and R. F. Ismagilov, *Adv. Mater.*, 2004, **16**, 1365.
14 E. Brouzes, M. Medkova, N. Savenelli, D. Marran, M. Twardowski, J. B. Hutchison, J. M. Rothberg, D. R. Link, N. Perrimon and M. L. Samuels, *Proc. Natl. Acad. Sci. U. S. A.*, 2009, **106**, 14195.
15 J. J. Agresti, E. Antipov, A. R. Abate, K. Ahn, A. C. Rowat, J. C. Baret, M. Marquez, A. M. Klibanov, A. D. Griffiths and D. A. Weitz, *Proc. Natl. Acad. Sci. U. S. A.*, 2010, **107**, 4004.
16 A. B. Theberge, F. Courtois, Y. Schaerli, M. Fischlechner, C. Abell, F. Hollfelder and W. T. Huck, *Angew. Chem., Int. Ed.*, 2010, **49**, 5846.
17 G. F. Christopher and S. L. Anna, *J. Phys. D: Appl. Phys.*, 2007, **40**, R319.
18 P. Garstecki, M. J. Fuerstman, H. A. Stone and G. M. Whitesides, *Lab Chip*, 2006, **6**, 693.
19 V. van Steijn, C. R. Kleijn and M. T. Kreutzer, *Lab Chip*, 2010, **10**, 2513.
20 M. De Menech, P. Garstecki, F. Jousse and H. A. Stone, *J. Fluid Mech.*, 2008, **595**, 141.
21 Y. N. Xia and G. M. Whitesides, *Annu. Rev. Mater. Sci.*, 1998, **28**, 153.

22 M. Abkarian, M. Faivre and H. A. Stone, *Proc. Natl. Acad. Sci. U. S. A.*, 2006, **103**, 538.
23 B. J. Adzima and S. S. Velankar, *J. Micromech. Microeng.*, 2006, **16**, 1504.
24 M. J. Fuerstman, A. Lai, M. E. Thurlow, S. S. Shevkoplyas, H. A. Stone and G. M. Whitesides, *Lab Chip*, 2007, **7**, 1479.
25 A. R. Abate and D. A. Weitz, *Appl. Phys. Lett.*, 2008, **92**, 243509.
26 S. A. Vanapalli, A. G. Banpurkar, D. van den Ende, M. H. G. Duits and F. Mugele, *Lab Chip*, 2009, **9**, 982.
27 D. A. Sessoms, A. Amon, L. Courbin and P. Panizza, *Phys. Rev. Lett.*, 2010, **105**, 154501.
28 V. Labrot, M. Schindler, P. Guillot, A. Colin and M. Joanicot, *Biomicrofluidics*, 2009, **3**, 012804.
29 P. Garstecki, H. A. Stone and G. M. Whitesides, *Phys. Rev. Lett.*, 2005, **94**, 164501.
30 G. F. Christopher, N. N. Noharuddin, J. A. Taylor and S. L. Anna, *Phys. Rev. E: Stat., Nonlinear, Soft Matter Phys.*, 2008, **78**, 036317.
31 H. H. Liu and Y. H. Zhang, *J. Appl. Phys.*, 2009, **106**, 034906.
32 A. S. Utada, A. Fernandez-Nieves, H. A. Stone and D. A. Weitz, *Phys. Rev. Lett.*, 2007, **99**, 094502.